

Decoupling Control of Parallel Manipulators

Thomas Dehaeze^{a,*}, Mohit Verma^b, Jennifer Watchi^c, Christophe Collette^c

^a*ESRF, The European Synchrotron, Grenoble, France*

^b*CSIR, Structural Engineering Research Centre, Taramani, Chennai, India.*

^c*Precision Mechatronics Laboratory, University of Liège, Belgium.*

Abstract

abstract

Keywords: singular value decomposition, decoupling, vibration isolation, active control

1. Introduction

The control of parallel manipulators (and any MIMO system in general) typically involves a two-step approach: first decoupling the plant dynamics (using various strategies discussed in this paper), followed by the application of SISO control for the decoupled plant.

When sensors are integrated within the struts, decentralized control may be applied, as the system is already well decoupled at low frequency. For instance, [1] implemented a system where each strut consists of piezoelectric stack actuators and eddy current displacement sensors, with separate PI controllers for each strut. A similar control architecture was proposed in [2] using strain gauge sensors integrated in each strut.

An alternative strategy involves decoupling the system in the Cartesian frame using Jacobian matrices. As demonstrated during the study of Stewart platform kinematics, Jacobian matrices can be utilized to map actuator forces to forces and torques applied on the top platform. This approach enables the implementation of controllers in a defined frame. It has been applied with various sensor types including force sensors [3], relative displacement sensors [4], and inertial sensors [5], [6]. The Cartesian frame in which the system is

*Corresponding author

Email address: thomas.dehaeze@esrf.fr (Thomas Dehaeze)

decoupled is typically chosen at the point of interest (i.e., where the motion is of interest) or at the center of mass.

Modal decoupling represents another noteworthy decoupling strategy, wherein the “local” plant inputs and outputs are mapped to the modal space. In this approach, multiple SISO plants, each corresponding to a single mode, can be controlled independently. This decoupling strategy has been implemented for active damping applications [7], which is logical as it is often desirable to dampen specific modes. The strategy has also been employed in [8] for vibration isolation purposes using geophones, and in [9] using force sensors.

Another completely different strategy would be to implement a multi-variable control directly on the coupled system. \mathcal{H}_∞ and μ -synthesis were applied to a Stewart platform model in [10]. In [11], decentralized force feedback was first applied, followed by \mathcal{H}_2 -synthesis for vibration isolation based on accelerometers. \mathcal{H}_∞ -synthesis was also employed in [12] for active damping based on accelerometers. A comparative study between \mathcal{H}_∞ -synthesis and decentralized control in the frame of the struts was performed in [13]. Their experimental closed-loop results indicated that the \mathcal{H}_∞ controller did not outperform the decentralized controller in the frame of the struts. These limitations were attributed to the model’s poor ability to predict off-diagonal dynamics, which is crucial for \mathcal{H}_∞ -synthesis.

The purpose of this paper is to compare several methods for the decoupling of parallel manipulators, an analysis that appears to be lacking in the literature. A simplified parallel manipulator model is introduced in Section 2 as a test case for evaluating decoupling strategies. The decentralized plant (transfer functions from actuators to sensors integrated in the struts) is examined in Section 3. Three approaches are investigated across subsequent sections: Jacobian matrix decoupling (Section 4), modal decoupling (Section 5), and Singular Value Decomposition (SVD) decoupling (Section 6). Finally, a comparative analysis with concluding observations is provided in Section 7.

2. Test Model

Instead of utilizing the Stewart platform for comparing decoupling strategies, a simplified parallel manipulator is employed to facilitate a more straightforward analysis. The system illustrated in Figure 1 is used for this purpose. It possesses three degrees of freedom (DoF) and incorporates three parallel

struts. Being a fully parallel manipulator, it is therefore quite similar to the Stewart platform.

Two reference frames are defined within this model: frame $\{M\}$ with origin O_M at the center of mass of the solid body, and frame $\{K\}$ with origin O_K at the center of stiffness of the parallel manipulator.

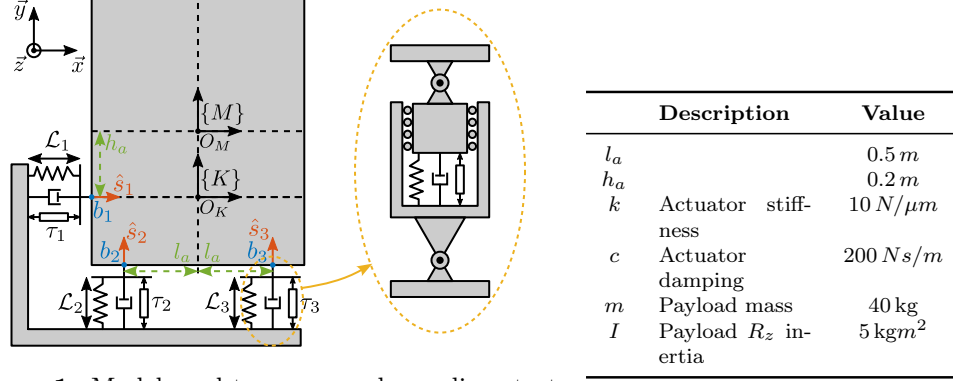


Figure 1: Model used to compare decoupling strategies

Table 1: Model parameters

The equations of motion are derived by applying Newton's second law to the suspended mass, expressed at its center of mass (1), where $\mathcal{X}_{\{M\}}$ represents the two translations and one rotation with respect to the center of mass, and $\mathcal{F}_{\{M\}}$ denotes the forces and torque applied at the center of mass.

$$M_{\{M\}} \ddot{\mathcal{X}}_{\{M\}}(t) = \sum \mathcal{F}_{\{M\}}(t), \quad \mathcal{X}_{\{M\}} = \begin{bmatrix} x \\ y \\ R_z \end{bmatrix}, \quad \mathcal{F}_{\{M\}} = \begin{bmatrix} F_x \\ F_y \\ M_z \end{bmatrix} \quad (1)$$

The Jacobian matrix $\mathbf{J}_{\{M\}}$ is employed to map the spring, damping, and actuator forces to XY forces and Z torque expressed at the center of mass (2).

$$\mathbf{J}_{\{M\}} = \begin{bmatrix} 1 & 0 & h_a \\ 0 & 1 & -l_a \\ 0 & 1 & l_a \end{bmatrix} \quad (2)$$

Subsequently, the equation of motion relating the actuator forces τ to the motion of the mass $\mathcal{X}_{\{M\}}$ is derived (3).

$$M_{\{M\}} \ddot{\mathcal{X}}_{\{M\}}(t) + \mathbf{J}_{\{M\}}^T \mathbf{C} \mathbf{J}_{\{M\}} \dot{\mathcal{X}}_{\{M\}}(t) + \mathbf{J}_{\{M\}}^T \mathbf{K} \mathbf{J}_{\{M\}} \mathcal{X}_{\{M\}}(t) = \mathbf{J}_{\{M\}}^T \boldsymbol{\tau}(t) \quad (3)$$

The matrices representing the payload inertia, actuator stiffness, and damping are shown in (4).

$$\mathbf{M}_{\{M\}} = \begin{bmatrix} m & 0 & 0 \\ 0 & m & 0 \\ 0 & 0 & I \end{bmatrix}, \quad \mathbf{K} = \begin{bmatrix} k & 0 & 0 \\ 0 & k & 0 \\ 0 & 0 & k \end{bmatrix}, \quad \mathbf{C} = \begin{bmatrix} c & 0 & 0 \\ 0 & c & 0 \\ 0 & 0 & c \end{bmatrix} \quad (4)$$

The parameters employed for the subsequent analysis are summarized in Table 1, which includes values for geometric parameters (l_a , h_a), mechanical properties (actuator stiffness k and damping c), and inertial characteristics (payload mass m and rotational inertia I).

3. Control in the frame of the struts

The dynamics in the frame of the struts are first examined. The equation of motion relating actuator forces $\boldsymbol{\tau}$ to strut relative motion $\boldsymbol{\mathcal{L}}$ is derived from equation (3) by mapping the Cartesian motion of the mass to the relative motion of the struts using the Jacobian matrix $\mathbf{J}_{\{M\}}$ defined in (2). The obtained transfer function from $\boldsymbol{\tau}$ to $\boldsymbol{\mathcal{L}}$ is shown in (5).

$$\frac{\boldsymbol{\mathcal{L}}}{\boldsymbol{\tau}}(s) = \mathbf{G}_{\mathcal{L}}(s) = \left(\mathbf{J}_{\{M\}}^{-\top} \mathbf{M}_{\{M\}} \mathbf{J}_{\{M\}}^{-1} s^2 + \mathbf{C}s + \mathbf{K} \right)^{-1} \quad (5)$$

At low frequencies, the plant converges to a diagonal constant matrix whose diagonal elements are equal to the actuator stiffnesses (6). At high frequencies, the plant converges to the mass matrix mapped in the frame of the struts, which is generally highly non-diagonal.

$$\mathbf{G}_{\mathcal{L}}(j\omega) \xrightarrow[\omega \rightarrow 0]{} \mathbf{K}^{-1} \quad (6)$$

The magnitude of the coupled plant $\mathbf{G}_{\mathcal{L}}$ is illustrated in Figure 2. This representation confirms that at low frequencies (below the first suspension mode), the plant is well decoupled. Depending on the symmetry present in the system, certain diagonal elements may exhibit identical values, as demonstrated for struts 2 and 3 in this example.

4. Jacobian Decoupling

4.1. Jacobian Matrix

The Jacobian matrix $\mathbf{J}_{\{O\}}$ serves a dual purpose in the decoupling process: it converts strut velocity $\dot{\boldsymbol{\mathcal{L}}}$ to payload velocity and angular velocity $\dot{\boldsymbol{\mathcal{X}}}_{\{O\}}$,

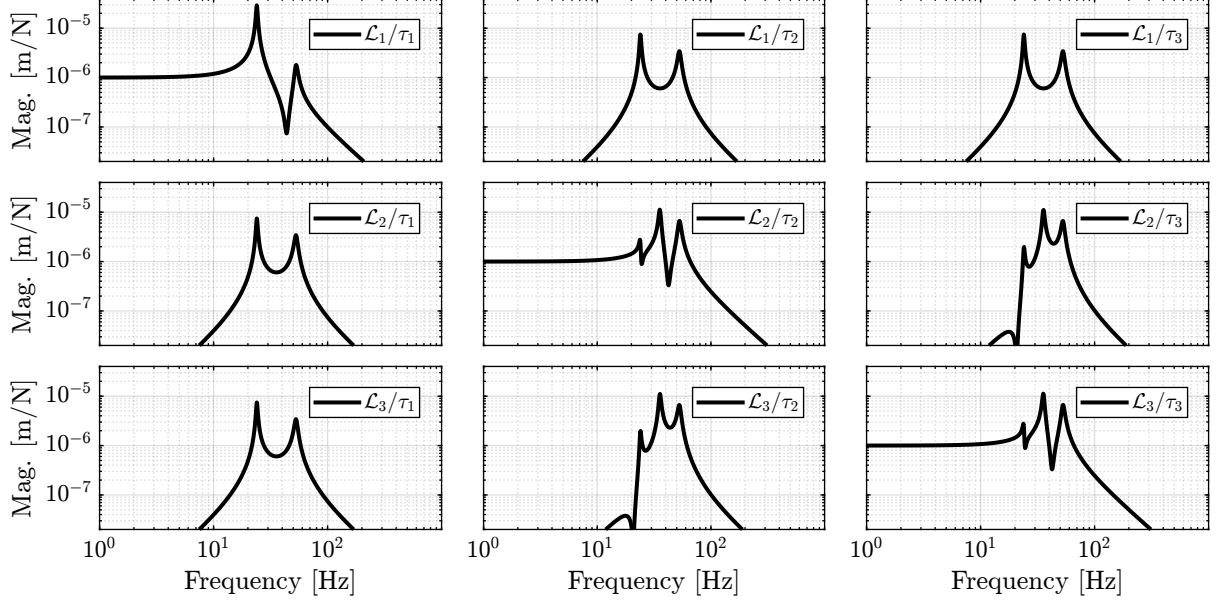


Figure 2: Model dynamics from actuator forces to relative displacement sensor of each strut.

and it transforms actuator forces τ to forces/torque applied on the payload $\mathcal{F}_{\{O\}}$, as expressed in equation (7).

$$\dot{\mathcal{X}}_{\{O\}} = J_{\{O\}} \dot{\mathcal{L}}, \quad \dot{\mathcal{L}} = J_{\{O\}}^{-1} \dot{\mathcal{X}}_{\{O\}} \quad (7a)$$

$$\mathcal{F}_{\{O\}} = J_{\{O\}}^T \tau, \quad \tau = J_{\{O\}}^{-T} \mathcal{F}_{\{O\}} \quad (7b)$$

The resulting plant (Figure 3) have inputs and outputs with clear physical interpretations:

- $\mathcal{F}_{\{O\}}$ represents forces/torques applied on the payload at the origin of frame $\{O\}$
- $\mathcal{X}_{\{O\}}$ represents translations/rotation of the payload expressed in frame $\{O\}$

The transfer function from $\mathcal{F}_{\{O\}}$ to $\mathcal{X}_{\{O\}}$, denoted $\mathbf{G}_{\{O\}}(s)$ can be computed using (8).

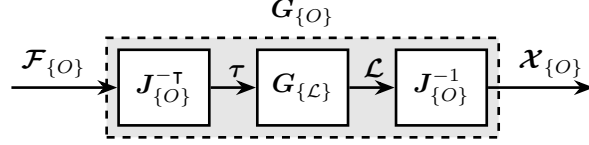


Figure 3: Block diagram of the transfer function from $\mathcal{F}_{\{O\}}$ to $\mathcal{X}_{\{O\}}$

$$\frac{\mathcal{X}_{\{O\}}}{\mathcal{F}_{\{O\}}}(s) = \mathbf{G}_{\{O\}}(s) = \left(\mathbf{J}_{\{O\}}^{\top} \mathbf{J}_{\{M\}}^{-\top} \mathbf{M}_{\{M\}} \mathbf{J}_{\{M\}}^{-1} \mathbf{J}_{\{O\}} s^2 + \mathbf{J}_{\{O\}}^{\top} \mathbf{C} \mathbf{J}_{\{O\}} s + \mathbf{J}_{\{O\}}^{\top} \mathbf{K} \mathbf{J}_{\{O\}} \right)^{-1} \quad (8)$$

The frame $\{O\}$ can be selected according to specific requirements, but the decoupling properties are significantly influenced by this choice. Two natural reference frames are particularly relevant: the center of mass and the center of stiffness.

4.2. Center Of Mass

When the decoupling frame is located at the center of mass (frame $\{M\}$ in Figure 1), the Jacobian matrix and its inverse are expressed as in (9).

$$\mathbf{J}_{\{M\}} = \begin{bmatrix} 1 & 0 & h_a \\ 0 & 1 & -l_a \\ 0 & 1 & l_a \end{bmatrix}, \quad \mathbf{J}_{\{M\}}^{-1} = \begin{bmatrix} 1 & \frac{h_a}{2l_a} & \frac{-h_a}{2l_a} \\ 0 & \frac{1}{2} & \frac{1}{2} \\ 0 & \frac{-1}{2l_a} & \frac{1}{2l_a} \end{bmatrix} \quad (9)$$

Analytical formula of the plant $\mathbf{G}_{\{M\}}(s)$ is derived (10).

$$\frac{\mathcal{X}_{\{M\}}}{\mathcal{F}_{\{M\}}}(s) = \mathbf{G}_{\{M\}}(s) = \left(\mathbf{M}_{\{M\}} s^2 + \mathbf{J}_{\{M\}}^{\top} \mathbf{C} \mathbf{J}_{\{M\}} s + \mathbf{J}_{\{M\}}^{\top} \mathbf{K} \mathbf{J}_{\{M\}} \right)^{-1} \quad (10)$$

At high frequencies, the plant converges to the inverse of the mass matrix, which is a diagonal matrix (11).

$$\mathbf{G}_{\{M\}}(j\omega) \xrightarrow{\omega \rightarrow \infty} -\omega^2 \mathbf{M}_{\{M\}}^{-1} = -\omega^2 \begin{bmatrix} 1/m & 0 & 0 \\ 0 & 1/m & 0 \\ 0 & 0 & 1/I \end{bmatrix} \quad (11)$$

Consequently, the plant exhibits effective decoupling at frequencies above the highest suspension mode as shown in Figure 4a. This strategy is typically

employed in systems with low-frequency suspension modes [14], where the plant approximates decoupled mass lines.

The low-frequency coupling observed in this configuration has a clear physical interpretation. When a static force is applied at the center of mass, the suspended mass rotates around the center of stiffness. This rotation is due to torque induced by the stiffness of the first actuator (i.e. the one on the left side), which is not aligned with the force application point. This phenomenon is illustrated in Figure 4b.

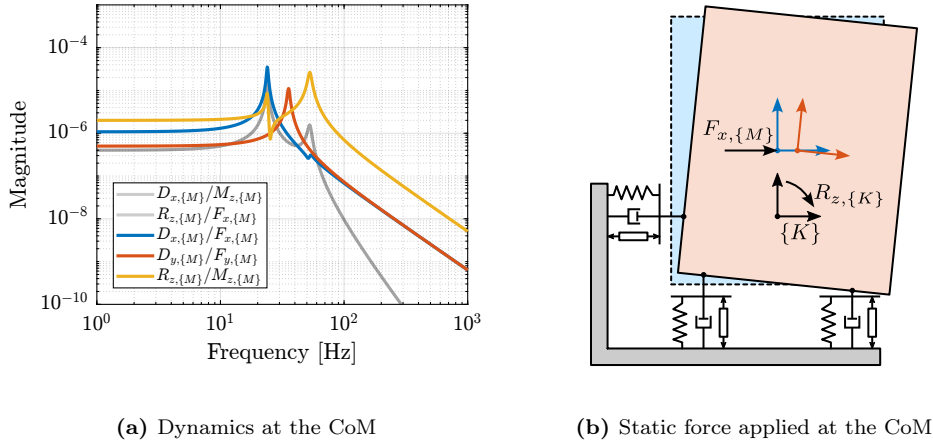


Figure 4: Plant decoupled using the Jacobian matrix expressed at the center of mass (a). The physical reason for low frequency coupling is illustrated in (b).

4.3. Center Of Stiffness

When the decoupling frame is located at the center of stiffness, the Jacobian matrix and its inverse are expressed as in (12).

$$\mathbf{J}_{\{K\}} = \begin{bmatrix} 1 & 0 & 0 \\ 0 & 1 & -l_a \\ 0 & 1 & l_a \end{bmatrix}, \quad \mathbf{J}_{\{K\}}^{-1} = \begin{bmatrix} 1 & 0 & 0 \\ 0 & \frac{1}{2} & \frac{1}{2} \\ 0 & \frac{-1}{2l_a} & \frac{1}{2l_a} \end{bmatrix} \quad (12)$$

The frame $\{K\}$ was selected based on physical reasoning, positioned in line with the side strut and equidistant between the two vertical struts. However, it could alternatively be determined through analytical methods to ensure that $\mathbf{J}_{\{K\}}^T \mathbf{K} \mathbf{J}_{\{K\}}$ forms a diagonal matrix. It should be noted that the existence of such a center of stiffness (i.e. a frame $\{K\}$ for which $\mathbf{J}_{\{K\}}^T \mathbf{K} \mathbf{J}_{\{K\}}$ is diagonal) is not guaranteed for arbitrary systems. This property is typically

achievable only in systems exhibiting specific symmetrical characteristics, as is the case in the present example.

The analytical expression for the plant in this configuration was then computed (13).

$$\frac{\mathcal{X}_{\{K\}}}{\mathcal{F}_{\{K\}}}(s) = \mathbf{G}_{\{K\}}(s) = \left(\mathbf{J}_{\{K\}}^\top \mathbf{J}_{\{M\}}^{-\top} \mathbf{M}_{\{M\}} \mathbf{J}_{\{M\}}^{-1} \mathbf{J}_{\{K\}} s^2 + \mathbf{J}_{\{K\}}^\top \mathbf{C} \mathbf{J}_{\{K\}} s + \mathbf{J}_{\{K\}}^\top \mathbf{K} \mathbf{J}_{\{K\}} \right)^{-1} \quad (13)$$

Figure 5 presents the dynamics of the plant when decoupled using the Jacobian matrix expressed at the center of stiffness. The plant is well decoupled below the suspension mode with the lowest frequency (14), making it particularly suitable for systems with high stiffness.

$$\mathbf{G}_{\{K\}}(j\omega) \xrightarrow{\omega \rightarrow 0} \mathbf{J}_{\{K\}}^{-1} \mathbf{K}^{-1} \mathbf{J}_{\{K\}}^{-\top} \quad (14)$$

The physical reason for high-frequency coupling is illustrated in Figure 5b. When a high-frequency force is applied at a point not aligned with the center of mass, it induces rotation around the center of mass.

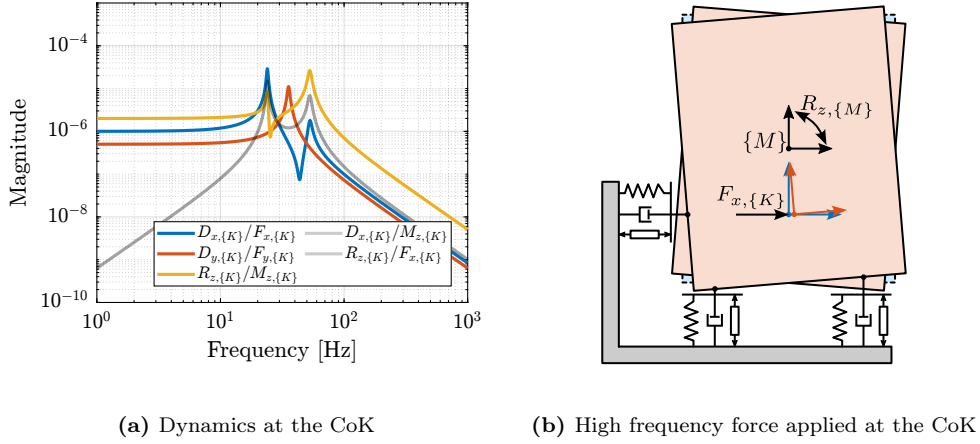


Figure 5: Plant decoupled using the Jacobian matrix expressed at the center of stiffness (a). The physical reason for high frequency coupling is illustrated in (b).

5. Modal Decoupling

Modal decoupling represents an approach based on the principle that a mechanical system's behavior can be understood as a combination of con-

tributions from various modes [15]. To convert the dynamics in the modal space, the equation of motion are first written with respect to the center of mass (15).

$$\mathbf{M}_{\{M\}}\ddot{\mathbf{x}}_{\{M\}}(t) + \mathbf{C}_{\{M\}}\dot{\mathbf{x}}_{\{M\}}(t) + \mathbf{K}_{\{M\}}\mathbf{x}_{\{M\}}(t) = \mathbf{J}_{\{M\}}^T\boldsymbol{\tau}(t) \quad (15)$$

For modal decoupling, a change of variables is introduced (16) where \mathbf{x}_m represents the modal amplitudes and Φ is a $n \times n$ ¹ matrix whose columns correspond to the mode shapes of the system, computed from $\mathbf{M}_{\{M\}}$ and $\mathbf{K}_{\{M\}}$.

$$\mathbf{x}_{\{M\}} = \Phi\mathbf{x}_m \quad (16)$$

By pre-multiplying equation (15) by Φ^T and applying the change of variable (16), a new set of equations of motion is obtained (17) where $\boldsymbol{\tau}_m$ represents the modal input, while \mathbf{M}_m , \mathbf{C}_m , and \mathbf{K}_m denote the modal mass, damping, and stiffness matrices respectively.

$$\underbrace{\Phi^T\mathbf{M}\Phi}_{\mathbf{M}_m}\ddot{\mathbf{x}}_m(t) + \underbrace{\Phi^T\mathbf{C}\Phi}_{\mathbf{C}_m}\dot{\mathbf{x}}_m(t) + \underbrace{\Phi^T\mathbf{K}\Phi}_{\mathbf{K}_m}\mathbf{x}_m(t) = \underbrace{\Phi^T\mathbf{J}^T\boldsymbol{\tau}(t)}_{\boldsymbol{\tau}_m(t)} \quad (17)$$

The inherent mathematical structure of the mass, damping, and stiffness matrices [16, chapt. 8] ensures that modal matrices are diagonal [17, chapt. 2.3]. This diagonalization transforms equation (17) into a set of n decoupled equations, enabling independent control of each mode without cross-interaction.

To implement this approach from a decentralized plant, the architecture shown in Figure 6 is employed. Inputs of the decoupling plant are the modal modal inputs $\boldsymbol{\tau}_m$ and the outputs are the modal amplitudes \mathbf{x}_m . This implementation requires knowledge of the system's equations of motion, from which the mode shapes matrix Φ is derived. The resulting decoupled system features diagonal elements each representing second-order resonant systems that are straightforward to control individually.

Modal decoupling was then applied to the test model. First, the eigenvectors Φ of $\mathbf{M}_{\{M\}}^{-1}\mathbf{K}_{\{M\}}$ were computed (18). While analytical derivation of

¹ n corresponds to the number of degrees of freedom, here $n = 3$

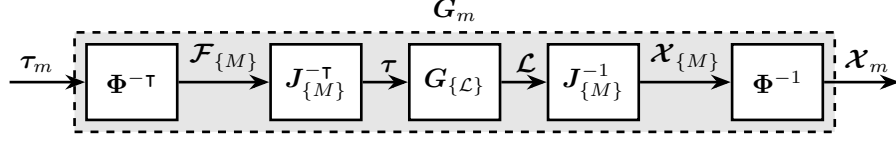


Figure 6: Modal Decoupling Architecture

eigenvectors could be obtained for such a simple system, they are typically computed numerically for practical applications.

$$\Phi = \begin{bmatrix} \frac{I-h_a^2m-2l_a^2m-\alpha}{2h_am} & 0 & \frac{I-h_a^2m-2l_a^2m+\alpha}{2h_am} \\ 0 & 1 & 0 \\ 1 & 0 & 1 \end{bmatrix}, \quad \alpha = \sqrt{(I + m(h_a^2 - 2l_a^2))^2 + 8m^2h_a^2l_a^2} \quad (18)$$

The numerical values for the eigenvector matrix and its inverse are shown in (19).

$$\Phi = \begin{bmatrix} -0.905 & 0 & -0.058 \\ 0 & 1 & 0 \\ 0.424 & 0 & -0.998 \end{bmatrix}, \quad \Phi^{-1} = \begin{bmatrix} -1.075 & 0 & 0.063 \\ 0 & 1 & 0 \\ -0.457 & 0 & -0.975 \end{bmatrix} \quad (19)$$

The two computed matrices were implemented in the control architecture of Figure 6, resulting in three distinct second order plants as depicted in Figure 7a. Each of these diagonal elements corresponds to a specific mode, as shown in Figure 7b, resulting in a perfectly decoupled system.

6. SVD Decoupling

6.1. Singular Value Decomposition

Singular Value Decomposition (SVD) represents a powerful mathematical tool with extensive applications in data analysis [18, chapt. 1] and multivariable control systems where it is particularly valuable for analyzing directional properties in multivariable systems [19].

The SVD constitutes a unique matrix decomposition applicable to any complex matrix $\mathbf{X} \in \mathbb{C}^{n \times m}$, expressed as:

$$\mathbf{X} = \mathbf{U}\mathbf{\Sigma}\mathbf{V}^H \quad (20)$$

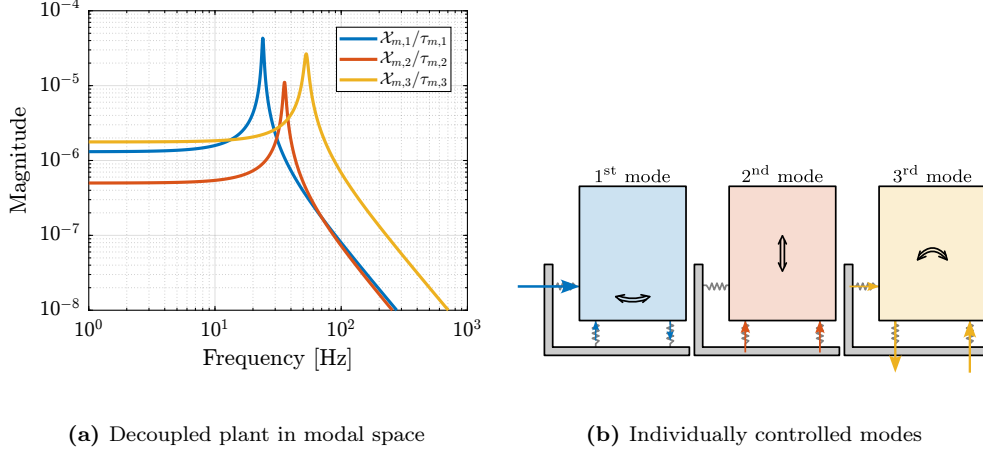


Figure 7: Plant using modal decoupling consists of second order plants (a) which can be used to individually address different modes illustrated in (b)

where $\mathbf{U} \in \mathbb{C}^{n \times n}$ and $\mathbf{V} \in \mathbb{C}^{m \times m}$ are unitary matrices with orthonormal columns, and $\mathbf{\Sigma} \in \mathbb{R}^{n \times n}$ is a diagonal matrix with real, non-negative entries. For real matrices \mathbf{X} , the resulting \mathbf{U} and \mathbf{V} matrices are also real, making them suitable for decoupling applications.

6.2. Decoupling using the SVD

The procedure for SVD-based decoupling begins with identifying the system dynamics from inputs to outputs, typically represented as a Frequency Response Function (FRF), which yields a complex matrix $\mathbf{G}(\omega_i)$ for multiple frequency points ω_i . A specific frequency is then selected for optimal decoupling, with the targeted crossover frequency ω_c often serving as an appropriate choice.

Since real matrices are required for the decoupling transformation, a real approximation of the complex measured response at the selected frequency must be computed. In this work, the method proposed in [20] was used as it preserves maximal orthogonality in the directional properties of the input complex matrix.

Following this approximation, a real matrix $\tilde{\mathbf{G}}(\omega_c)$ is obtained, and SVD is performed on this matrix. The resulting (real) unitary matrices \mathbf{U} and \mathbf{V} are structured such that $\mathbf{V}^{-\top} \tilde{\mathbf{G}}(\omega_c) \mathbf{U}^{-1}$ forms a diagonal matrix. These singular input and output matrices are then applied to decouple the system as illustrated in Figure 8, and the decoupled plant is described by (21).

$$\mathbf{G}_{\text{SVD}}(s) = \mathbf{U}^{-1} \mathbf{G}_{\{\mathcal{L}\}}(s) \mathbf{V}^{-\top} \quad (21)$$

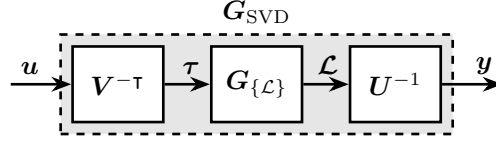


Figure 8: Decoupled plant \mathbf{G}_{SVD} using the Singular Value Decomposition

Implementation of SVD decoupling requires access to the system's FRF, at least in the vicinity of the desired decoupling frequency. This information can be obtained either experimentally or derived from a model. While this approach ensures effective decoupling near the chosen frequency, it provides no guarantees regarding decoupling performance away from this frequency. Furthermore, the quality of decoupling depends significantly on the accuracy of the real approximation, potentially limiting its effectiveness for plants with high damping.

6.3. Example

Plant decoupling using the Singular Value Decomposition was then applied on the test model. A decoupling frequency of 100 Hz was used. The plant response at that frequency, as well as its real approximation and the obtained \mathbf{U} and \mathbf{V} matrices are shown in (22).

$$\begin{aligned} \mathbf{G}_{\{\mathcal{L}\}}(\omega_c = 2\pi \cdot 100) &= 10^{-9} \begin{bmatrix} -99 - j2.6 & 74 + j4.2 & -74 - j4.2 \\ 74 + j4.2 & -247 - j9.7 & 102 + j7.0 \\ -74 - j4.2 & 102 + j7.0 & -247 - j9.7 \end{bmatrix} \\ \xrightarrow[\text{approximation}]{\text{real}} \tilde{\mathbf{G}}_{\{\mathcal{L}\}}(\omega_c) &= 10^{-9} \begin{bmatrix} -99 & 74 & -74 \\ 74 & -247 & 102 \\ -74 & 102 & -247 \end{bmatrix} \\ \xrightarrow{\text{SVD}} \mathbf{U} &= \begin{bmatrix} 0.34 & 0 & 0.94 \\ -0.66 & 0.71 & 0.24 \\ 0.66 & 0.71 & -0.24 \end{bmatrix}, \quad \mathbf{V} = \begin{bmatrix} -0.34 & 0 & -0.94 \\ 0.66 & -0.71 & -0.24 \\ -0.66 & -0.71 & 0.24 \end{bmatrix} \end{aligned} \quad (22)$$

Using these \mathbf{U} and \mathbf{V} matrices, the decoupled plant is computed according to equation (21). The resulting plant, depicted in Figure 9, exhibits

remarkable decoupling across a broad frequency range, extending well beyond the vicinity of ω_c . Additionally, the diagonal terms manifest as second-order dynamic systems, facilitating straightforward controller design.

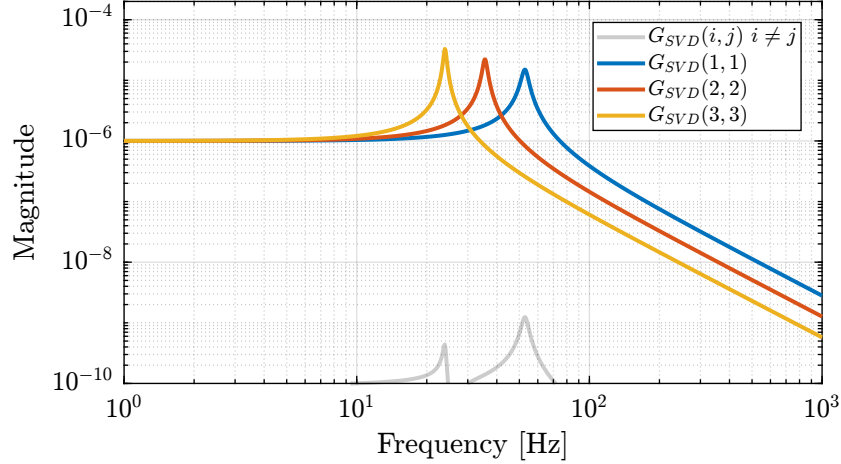
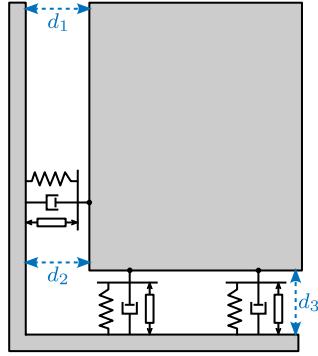


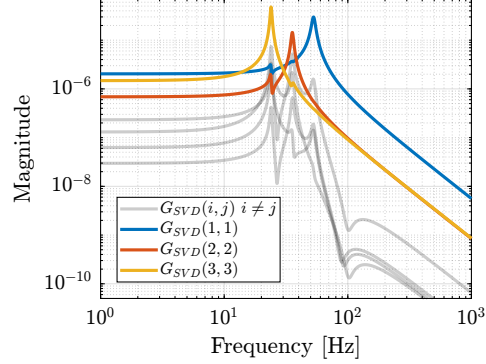
Figure 9: Plant dynamics $\mathbf{G}_{SVD}(s)$ obtained after decoupling using Singular Value Decomposition

As it was surprising to obtain such a good decoupling at all frequencies, a variant system with identical dynamics but different sensor configurations was examined. Instead of using relative motion sensors collocated with the struts, three relative motion sensors were positioned as shown in Figure 10a. Although Jacobian matrices could theoretically be used to map these sensors to the frame of the struts, application of the same SVD decoupling procedure yielded the plant response shown in Figure 10b, which exhibits significantly greater coupling. Notably, the coupling demonstrates local minima near the decoupling frequency, consistent with the fact that the decoupling matrices were derived specifically for that frequency point.

The exceptional performance of SVD decoupling on the plant with collocated sensors warrants further investigation. This effectiveness may be attributed to the symmetrical properties of the plant, as evidenced in the Bode plots of the decentralized plant shown in Figure 2. The phenomenon potentially relates to previous research on SVD controllers applied to systems with specific symmetrical characteristics [21].



(a) Alternative location of sensors



(b) Obtained decoupled plant

Figure 10: Application of SVD decoupling on a system schematically shown in (a). The obtained decoupled plant is shown in (b).

7. Comparison of decoupling strategies

While the three proposed decoupling methods may appear similar in their mathematical implementation (each involving pre-multiplication and post-multiplication of the plant with constant matrices), they differ significantly in their underlying approaches and practical implications, as summarized in Table 2.

Each method employs a distinct conceptual framework: Jacobian decoupling is “topology-driven”, relying on the geometric configuration of the system; modal decoupling is “physics-driven”, based on the system’s dynamical equations; and SVD decoupling is “data-driven”, utilizing measured frequency response functions.

The physical interpretation of decoupled plant inputs and outputs varies considerably among these methods. With Jacobian decoupling, inputs and outputs retain clear physical meaning, corresponding to forces/torques and translations/rotations in a specified reference frame. Modal decoupling arranges inputs to excite individual modes, with outputs combined to measure these modes separately. For SVD decoupling, inputs and outputs represent special directions ordered by decreasing controllability and observability at the chosen frequency, though physical interpretation becomes challenging for parallel manipulators.

This difference in interpretation relates directly to the “control space” in which the controllers operate. When these “control spaces” meaningfully

relate to the control objectives, controllers can be tuned to directly match specific requirements. For Jacobian decoupling, the controller typically operates in a frame positioned at the point where motion needs to be controlled, for instance where the light is focused in the NASS application. Modal decoupling provides a natural framework when specific vibrational modes require targeted control. SVD decoupling generally results in a loss of physical meaning for the “control space”, potentially complicating the process of relating controller design to practical system requirements.

The quality of decoupling achieved through these methods also exhibits distinct characteristics. Jacobian decoupling performance depends on the chosen reference frame, with optimal decoupling at low frequencies when aligned at the center of stiffness, or at high frequencies when aligned with the center of mass. Systems designed with coincident centers of mass and stiffness may achieve excellent decoupling using this approach. Modal decoupling offers good decoupling across all frequencies, though its effectiveness relies on the model accuracy, with discrepancies potentially resulting in significant off-diagonal elements. SVD decoupling can be implemented using measured data without requiring a model, with optimal performance near the chosen decoupling frequency, though its effectiveness may diminish at other frequencies and depends on the quality of the real approximation of the response at the selected frequency point.

8. Acknowledgments

References

- [1] K. Furutani, M. Suzuki, and R. Kudoh, “Nanometre-cutting machine using a stewart-platform parallel mechanism,” *Measurement Science and Technology*, vol. 15, no. 2, pp. 467–474, 2004 (cit. on p. 1).
- [2] Z. Du, R. Shi, and W. Dong, “A piezo-actuated high-precision flexible parallel pointing mechanism: Conceptual design, development, and experiments,” *IEEE Transactions on Robotics*, vol. 30, no. 1, pp. 131–137, 2014 (cit. on p. 1).
- [3] J. E. McInroy and J. C. Hamann, “Design and control of flexure jointed hexapods,” *IEEE Transactions on Robotics and Automation*, vol. 16, no. 4, pp. 372–381, 2000 (cit. on p. 1).

Table 2: Comparison of decoupling strategies

	Jacobian	Modal	SVD
Philosophy	Topology Driven	Physics Driven	Data Driven
Requirements	Known geometry	Known equations of motion	Identified FRF
Decoupling Matrices	Jacobian matrix $\mathbf{J}_{\{O\}}$	Eigenvectors Φ	SVD matrices \mathbf{U} and \mathbf{V}
Decoupled Plant	$\mathbf{G}_{\{O\}}(s)$ $\mathbf{J}_{\{O\}}^{-1} \mathbf{G}_{\mathcal{L}}(s) \mathbf{J}_{\{O\}}^{-\top}$	$\mathbf{G}_m(s)$ $\Phi^{-1} \mathbf{G}_{\mathcal{X}}(s) \Phi^{-\top}$	$\mathbf{G}_{\text{SVD}}(s)$ $\mathbf{U}^{-1} \mathbf{G}(s) \mathbf{V}^{-\top}$
Controller	$\mathbf{K}_{\{O\}}(s)$ $\mathbf{J}_{\{O\}}^{-\top} \mathbf{K}_d(s) \mathbf{J}_{\{O\}}^{-1}$	$\mathbf{K}_m(s)$ $\Phi^{-\top} \mathbf{K}_d(s) \Phi^{-1}$	$\mathbf{K}_{\text{SVD}}(s)$ $\mathbf{V}^{-\top} \mathbf{K}_d(s) \mathbf{U}^{-1}$
Interpretation	Forces/Torques to Displacement/Rotation in chosen frame	Inputs (resp. outputs) to excite (resp. sense) individual modes	Directions of max to min controllability/observability
Effectiveness	Decoupling at low or high frequency depending on the chosen frame	Good decoupling at all frequencies	Good decoupling near the chosen frequency
Pros	Retain physical meaning of inputs / outputs. Controller acts on a meaningfully “frame”	Ability to target specific modes. Simple 2^{nd} order diagonal plants	Good Decoupling near the crossover. Very General and requires no model
Cons	Good decoupling at all frequency can only be obtained for specific mechanical architecture	Relies on the accuracy of equation of motions. Robustness to unmodelled dynamics may be poor	Loss of physical meaning of inputs / outputs. Decoupling away from the chosen frequency may be poor

- [4] D. H. Kim, J.-Y. Kang, and K.-I. Lee, “Robust tracking control design for a 6 dof parallel manipulator,” *Journal of Robotic Systems*, vol. 17, no. 10, pp. 527–547, 2000 (cit. on p. 2).
- [5] X. Li, J. C. Hamann, and J. E. McInroy, “Simultaneous vibration isolation and pointing control of flexure jointed hexapods,” in *Smart Structures and Materials 2001: Smart Structures and Integrated Systems*, Aug. 2001 (cit. on p. 2).
- [6] H. Abbas and H. Hai, “Vibration isolation concepts for non-cubic stewart platform using modal control,” in *Proceedings of 11th International Bhurban Conference on Applied Sciences & Technology (IBCAST) Islamabad, Pakistan*, Jan. 2014 (cit. on p. 2).
- [7] J. Holterman and T. J. A. de Vries, “Active damping based on decoupled collocated control,” *IEEE/ASME Transactions on Mechatronics*, vol. 10, no. 2, pp. 135–145, 2005 (cit. on p. 2).
- [8] H. Pu, X. Chen, Z. Zhou, and X. Luo, “Six-degree-of-freedom active vibration isolation system with decoupled collocated control,” *Proceedings of the Institution of Mechanical Engineers, Part B: Journal of Engineering Manufacture*, vol. 226, no. 2, pp. 313–325, 2011 (cit. on p. 2).
- [9] X. Yang, H. Wu, B. Chen, S. Kang, and S. Cheng, “Dynamic modeling and decoupled control of a flexible stewart platform for vibration isolation,” *Journal of Sound and Vibration*, vol. 439, pp. 398–412, Jan. 2019 (cit. on p. 2).
- [10] L. Lei and W. Benli, “Multi objective robust active vibration control for flexure jointed struts of stewart platforms via H_∞ and μ synthesis,” *Chinese Journal of Aeronautics*, vol. 21, no. 2, pp. 125–133, 2008 (cit. on p. 2).
- [11] X. Xie, C. Wang, and Z. Zhang, “Modeling and control of a hybrid passive/active stewart vibration isolation platform,” in *INTER-NOISE and NOISE-CON Congress and Conference Proceedings*, Institute of Noise Control Engineering, vol. 255, 2017, pp. 1844–1853 (cit. on p. 2).
- [12] J. Jiao, Y. Wu, K. Yu, and R. Zhao, “Dynamic modeling and experimental analyses of stewart platform with flexible hinges,” *Journal of Vibration and Control*, vol. 25, no. 1, pp. 151–171, 2018 (cit. on p. 2).

- [13] D. Thayer, M. Campbell, J. Vagners, and A. von Flotow, “Six-axis vibration isolation system using soft actuators and multiple sensors,” *Journal of Spacecraft and Rockets*, vol. 39, no. 2, pp. 206–212, 2002 (cit. on p. 2).
- [14] H. Butler, “Position control in lithographic equipment,” *IEEE Control Systems*, vol. 31, no. 5, pp. 28–47, 2011 (cit. on p. 7).
- [15] A. M. Rankers, “Machine dynamics in mechatronic systems: An engineering approach,” Ph.D. dissertation, University of Twente, 1998 (cit. on p. 9).
- [16] G. F. Lang, “Understanding modal vectors,” in *Topics in Modal Analysis & Testing, Volume 10*. Springer, 2017, ch. 8, pp. 55–68 (cit. on p. 9).
- [17] A. Preumont, *Vibration Control of Active Structures - Fourth Edition* (Solid Mechanics and Its Applications). Springer International Publishing, 2018 (cit. on p. 9).
- [18] S. L. Brunton and J. N. Kutz, *Data-driven science and engineering: Machine learning, dynamical systems, and control*. Cambridge University Press, 2022 (cit. on p. 10).
- [19] S. Skogestad and I. Postlethwaite, *Multivariable Feedback Control: Analysis and Design - Second Edition*. John Wiley, 2007 (cit. on p. 10).
- [20] B. A. Kouvaritakis, “Theory and practice of the characteristic locus design method,” *Proceedings of the Institution of Electrical Engineers*, vol. 126, no. 6, p. 542, 1979 (cit. on p. 11).
- [21] M. Hovd, R. D. Braatz, and S. Skogestad, “SVD controllers for \mathcal{H}_2 -, \mathcal{H}_∞ - and μ -optimal control,” *Automatica*, vol. 33, no. 3, pp. 433–439, 1997 (cit. on p. 13).